

Learning spectral density functions in open quantum systems

Felipe Peleteiro¹,¹ João Victor Shiguetsugo Kawanami Lima¹,¹ Pedro Marcelo Prado¹,¹ Felipe Fernandes Fanchini¹,¹ and Ariel Norambuena^{2,*}

¹São Paulo State University (UNESP), School of Sciences, 17033-360, Bauru, SP, Brazil

²Departamento de Física, Universidad Técnica Federico Santa María, Casilla 110 V, Valparaíso, Chile

(Dated: March 2, 2026)

Spectral density functions quantify how environmental modes couple to quantum systems and govern their open dynamics. Inferring such frequency-dependent functions from time-domain measurements is an ill-conditioned inverse problem. Here, we use exactly solvable spin-boson models with pure-dephasing and amplitude-damping channels to reconstruct spectral density functions from noisy simulated data. First, we introduce a parameter estimation approach based on machine learning regressors to infer Lorentzian and Ohmic-like spectral density parameters, quantifying robustness to noise. Second, we show that a cosine transform inversion yields a physics-consistent spectral prior estimation, which is refined by a constrained neural network enforcing positivity and correct asymptotic behaviour. Our neural network framework robustly reconstructs structured spectral densities by filtering simulated noisy signals and learning general functional dependencies.

I. INTRODUCTION

In the theory of open quantum systems, the microscopic description of the environment introduces bath frequencies ω_k and the corresponding system-bath coupling constants $g_k \in \mathbb{C}$, where k may denote a discrete or continuous index. The spectral density function (SDF) is defined as $J(\omega) = \sum_k |g_k|^2 \delta(\omega - \omega_k)$ [1, 2], which encodes how environmental modes couple to the system under interest. The Dirac delta function $\delta(\omega - \omega_k)$ effectively models the environment as a continuous spectral distribution, facilitating analytical treatments for damping rates and time evolution. By construction, $J(\omega) \geq 0$, and the normalization condition $\int_0^\infty J(\omega) d\omega = \sum_k |g_k|^2$ must hold.

At low frequencies ($\omega \rightarrow 0$), density of states arguments or noise-correlation arguments typically lead to a power-law scaling $J(\omega) \propto \omega^s$ with $s \in \mathbb{R}^+$. Conversely, at high frequencies ($\omega \rightarrow \infty$), the SDF must decay, reflecting the suppression of high-energy bath excitations. The most widely used phenomenological model is the Ohmic-like SDF $J(\omega) = \alpha \omega_c^{1-s} \omega^s e^{-\omega/\omega_c}$, which captures the main physical features of a broad class of environments [3–5]. Here, $\alpha > 0$ sets the coupling strength, ω_c is the cutoff frequency, and s distinguishes sub-Ohmic ($s < 1$), Ohmic ($s = 1$), and super-Ohmic ($s > 1$) cases. While the Ohmic class enables analytical progress and provides valuable intuition, it fails to capture the complexity of structured environments, such as quantum dots [6] or solid-state spin defects in diamond [7, 8, 10].

Moving beyond phenomenological models, one may use *ab initio* calculations [7, 10] or molecular dynamics simulations [8, 9]. However, these approaches are computationally demanding, susceptible to discretization artifacts, and sensitive to many-body correlations. Alternatively, microscopic arguments within exactly solvable models can be invoked, although such methods remain restricted to specific scenarios, for instance, light-matter interactions in the electric-dipole approximation [1].

A promising direction is to estimate $J(\omega)$ directly from experimental data by combining artificial intelligence (AI) with physically consistent quantum models. Given a set of measurements, one may infer the SDF that best explains the observed dynamics under suitable constraints. Current AI-assisted strategies primarily employ neural networks to classify [13–15] or fit parameters [14] within the Ohmic class for the pure-dephasing spin-boson model. However, a systematic AI framework capable of reconstructing structured environments beyond Ohmic-like parametrizations from noisy data remains lacking. Moreover, robustness analyses indicate that small deviations in the SDF can lead to exponentially amplified errors in expectation values, highlighting the intrinsic sensitivity of this inverse quantum problem [16].

In this work, we present two complementary approaches to learn SDFs from time-domain data in exactly solvable spin-boson models, which we use to benchmark our results. The first performs AI-based parameter estimation within phenomenological spectral-density families using machine-learning regressors. The second exploits a cosine transform structure to construct a nonparametric spectral prior, which is subsequently stabilized by a physics-constrained neural network. We benchmark accuracy and robustness across noise regimes and discuss how these tools extend to broader classes of open quantum systems with known models.

II. MODELS

First, we consider the pure dephasing (PD) spin-boson model $\hat{H}_{\text{PD}} = \hat{H}_s + \hat{H}_b + \hat{V}_{\text{PD}}$, where $\hat{H}_s = (\omega_0/2)\hat{\sigma}_z \otimes \mathbb{1}_b$ describes a two-level system (TLS) with Bohr frequency ω_0 and $H_b = \mathbb{1}_s \otimes \sum_k \omega_k \hat{a}_k^\dagger \hat{a}_k$ is the bosonic bath. Here, $\sigma_z = |1\rangle\langle 1| - |0\rangle\langle 0|$ is the Pauli matrix in the TLS basis $\{|0\rangle, |1\rangle\}$, and \hat{a}_k (\hat{a}_k^\dagger) is the annihilation (creation) boson operator. The interaction Hamiltonian for the PD channel is given by ($\hbar = 1$)

$$\hat{V}_{\text{PD}} = \hat{\sigma}_z \otimes \sum_k \left(g_k \hat{a}_k + g_k^* \hat{a}_k^\dagger \right), \quad (1)$$

* ariel.norambuena@usm.cl

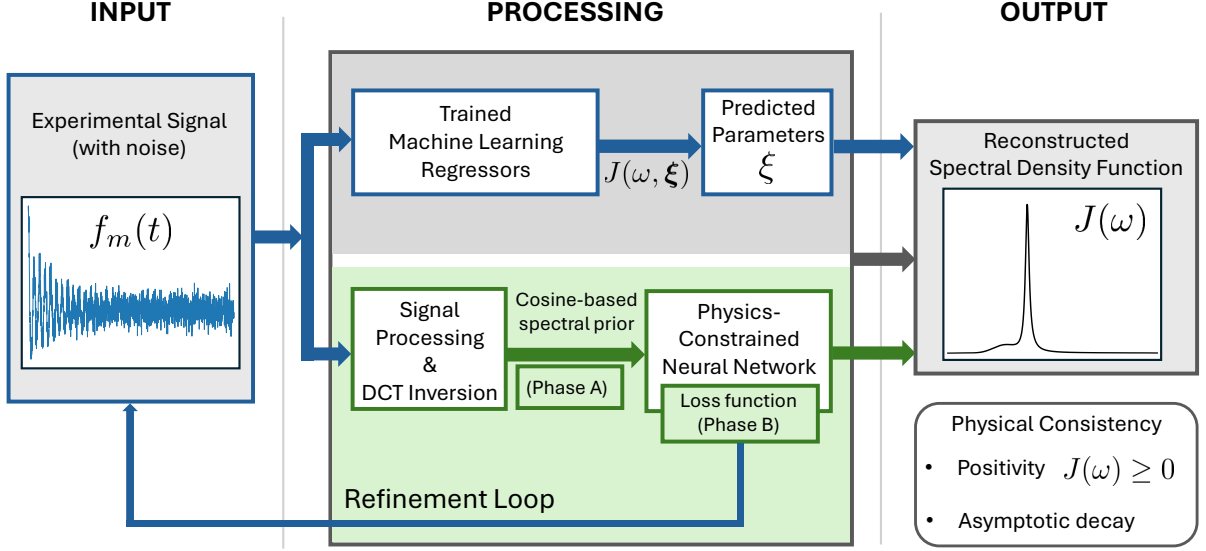


FIG. 1. Conceptual overview of the spectral density reconstruction problem. A quantum system coupled to a structured environment is characterized by a spectral density function $J(\omega)$, which determines measurable dynamical signals $f_m(t)$ through a known map $J(\omega) \mapsto f_m(t)$. The inverse problem, inferring $J(\omega)$ from noisy time-domain data, is ill-conditioned under finite time sampling and measurement noise. We address this challenge via two complementary AI-based strategies: (i) a parametric regression scheme for estimating SDF parameters, and (ii) a nonparametric approach combining discrete cosine transform (DCT) inversion with a constrained neural network refinement to obtain physically consistent spectral reconstructions.

where g_k are the coupling constants and the SDF is defined as

$$J(\omega) = \sum_k |g_k|^2 \delta(\omega - \omega_k). \quad (2)$$

The PD model captures the orbital-phonon dynamics in color centers [17] and time-invariant quantum discord [18], both of which describe Markovian and non-Markovian regimes. For a thermal bath state $\hat{\sigma}_b = e^{-\beta \hat{H}_b} / \text{Tr}[\exp(-\beta \hat{H}_b)]$ with $\beta = (k_B T)^{-1}$ the inverse temperature, the exact time-local Lindblad dynamics is $\dot{\hat{\rho}}_{\text{PD}} = (\gamma_{\text{PD}}(t)/2)[\hat{\sigma}_z \hat{\rho}_{\text{PD}} \hat{\sigma}_z - \hat{\rho}_{\text{PD}}]$ [18, 19]. Here, $\gamma_{\text{PD}}(t) = \int_0^\infty J(\omega) [2n(\omega) + 1] \sin(\omega t) d\omega$ is the time-dependent rate, where $n(\omega) = [\exp(\beta \hbar \omega) - 1]^{-1}$ is the mean boson number. Since populations remain constant in the PD model, the quantum coherence $C(t) = \sum_{i \neq j} |\rho_{ij}(t)|$ [20] is a natural observable. Experimentally, it can be reconstructed as

$$f_{\text{PD}}(t) = \sqrt{\langle \hat{\sigma}_x(t) \rangle^2 + \langle \hat{\sigma}_y(t) \rangle^2} = 2|\rho_{01}(0)|e^{-G(t)}, \quad (3)$$

$$G(t) = \int_0^\infty \frac{J(\omega)}{\omega^2} \coth\left(\frac{\beta\omega}{2}\right) [1 - \cos(\omega t)] d\omega, \quad (4)$$

where $f_{\text{PD}}(t) = C(t)$ is the quantum coherence signal for the PD model, with initial value $C(0) = 2|\rho_{01}(0)|$. Second, we consider the amplitude-damping (AD) spin-boson model, whose Hamiltonian is $\hat{H}_{\text{AD}} = \hat{H}_s + \hat{H}_b + \hat{V}_{\text{AD}}$, in which the system and bath Hamiltonians are the same as the PD model. In the rotating-wave approximation, the system-environment interaction Hamiltonian for the AD channel is given by ($\hbar =$

1)

$$\hat{V}_{\text{AD}} = \sum_k \left(g_k \hat{\sigma}_+ \otimes \hat{a}_k + g_k^* \hat{\sigma}_- \otimes \hat{a}_k^\dagger \right), \quad (5)$$

where $\hat{\sigma}_+ = (\hat{\sigma}_x + i\hat{\sigma}_y)/2$ and $\hat{\sigma}_- = (\hat{\sigma}_+)^{\dagger}$ describes absorption and emission processes, respectively.

We study spontaneous emission in the single-excitation manifold, where $\hat{N} = \hat{\sigma}_+ \hat{\sigma}_- + \sum_k \hat{a}_k^\dagger \hat{a}_k$ is the excitation number operator. Since the symmetry $[\hat{N}, \hat{H}_{\text{AD}}] = 0$, in the single-excitation manifold, we can decompose the wavefunction as $|\Psi(t)\rangle = c_0(t)|0\rangle \otimes |0_k\rangle + c_1(t)|1\rangle \otimes |0_k\rangle + \sum_k c_k(t)|0\rangle \otimes |1_k\rangle$. We use the initial product state $\hat{\rho}(0) = |1\rangle\langle 1| \otimes |0_k\rangle\langle 0_k|$, leading to the exact dynamics $\dot{\hat{\rho}}_{\text{AD}} = -iS(t)[\hat{\sigma}_+ \hat{\sigma}_-, \hat{\rho}_{\text{AD}}] + \gamma(t)[\hat{\sigma}_- \hat{\rho}_{\text{AD}} \hat{\sigma}_+ - (1/2)\{\hat{\sigma}_+ \hat{\sigma}_-, \hat{\rho}_{\text{AD}}\}]$, with $\hat{\rho}_{\text{AD}} = \text{Tr}_b[|\Psi(t)\rangle\langle\Psi(t)|]$, $S(t) = -\text{Im}\{\dot{c}_1(t)/c_1(t)\}$, and $\gamma(t) = -\text{Re}\{\dot{c}_1(t)/c_1(t)\}$ [2]. Since populations evolve in this model, a suitable observable is

$$f_{\text{AD}}(t) = \langle \hat{\sigma}_z \rangle = 2|c_1(t)|^2 - 1, \quad (6)$$

$$\dot{c}_1(t) = - \int_0^t K(t-\tau) c_1(\tau) d\tau, \quad (7)$$

$$K(t) = \int_0^\infty e^{i(\omega_0 - \omega)t} J(\omega) d\omega. \quad (8)$$

Equations (3) and (6) define a map $J(\omega) \mapsto f_m(t)$ with a model label $m \in \{\text{PD}, \text{AD}\}$; throughout, we address the corresponding inverse problem $f_m(t) \mapsto J(\omega)$. In general, for different open quantum systems the role of the SDF into observables can be derived as is explained in Appendix A. Maps

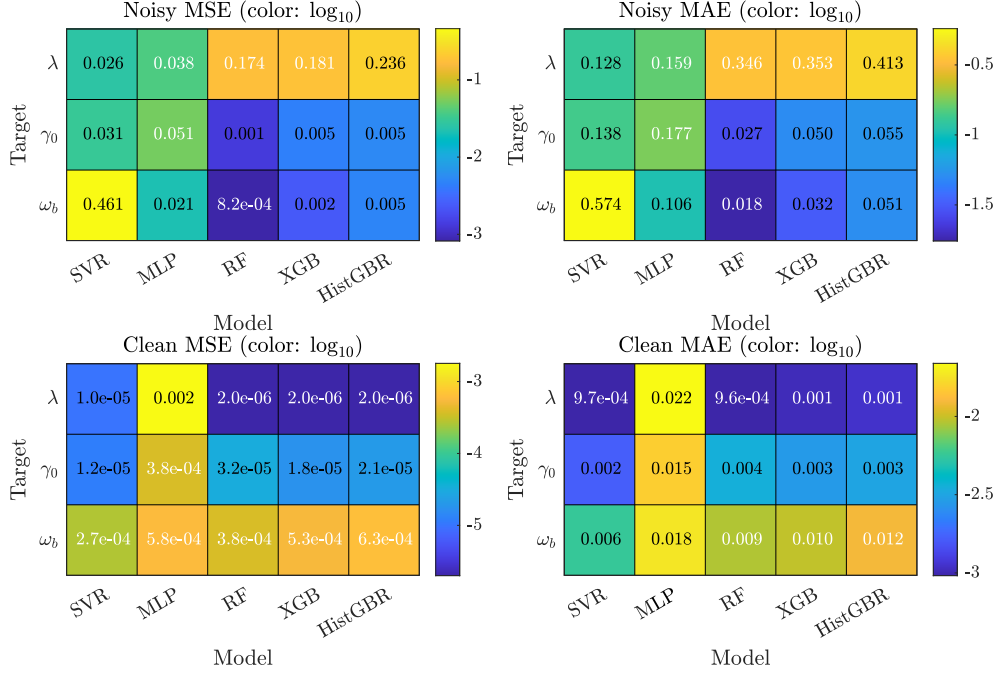


FIG. 2. Machine learning accuracy for parametric SDF inference in the amplitude-damping (AD) channel. Each row corresponds to a target parameter ($\lambda, \gamma_0, \omega_b$) and each column to a regression model. Colors show $\log_{10}(\text{MSE})$ and $\log_{10}(\text{MAE})$ for noisy (top) and noiseless (bottom) signals, highlighting robustness to measurement noise and model-dependent performance.

in open quantum systems are useful, as we shall illustrate later, for training and guiding optimization in AI-based models, as shown in the schematic overview in Fig. 1.

III. PHENOMENOLOGICAL MODELS AND PARAMETER ESTIMATION

We introduce parametrized families of SDFs, denoted by $J(\omega, \xi)$, with $\xi \in \mathbb{R}^p$ representing model parameters, where $p \geq 1$ is the parameter dimension. In our computational experiments, we use two known SDFs

$$J(\omega, \xi) = 2\alpha\omega_c^{1-s}\omega^s e^{-\omega/\omega_c} \quad \text{PD model,} \quad (9)$$

$$J(\omega, \xi) = \frac{1}{2\pi} \frac{\gamma_0\lambda^2}{(\omega - \omega_b)^2 + \lambda^2} \quad \text{AD model,} \quad (10)$$

where $\xi = [\alpha, s, \omega_c]$ corresponds to the Ohmic class and $\xi = [\gamma_0, \lambda, \omega_b]$ describes Lorentzian functions. Here, γ_0 is the amplitude, λ the width, and ω_b the bosonic frequency of the peak associated with the Lorentzian SDF. At zero temperature ($T = 0$), we obtain $f_{\text{PD}}(t) = 2|\rho_{10}(0)|\mathcal{F}_{\text{PD}}(t)$ and $f_{\text{AD}}(t) = 2\rho_{11}(0)\mathcal{F}_{\text{AD}}(t) - 1$, where analytical expressions for the signals are given by

$$\mathcal{F}_{\text{PD}}(t) = \exp\left(2\alpha\Gamma(s)\int_0^{\omega_c t} \frac{\sin(s \tan^{-1}(x))}{[1+x^2]^{s/2}} dx\right) \quad (11)$$

$$\mathcal{F}_{\text{AD}}(t) = \exp(-\lambda t) \left| \cosh\left(\frac{dt}{2}\right) + \frac{\Lambda}{d} \sinh\left(\frac{dt}{2}\right) \right|^2 \quad (12)$$

where $d = [\Lambda^2 - 4\gamma_0\lambda]^{1/2}$, $\Lambda = \lambda - i\delta$, $\delta = \omega_0 - \omega_b$ is the detuning, and $\Gamma(s)$ the Gamma function. The analytical expression of $\mathcal{F}_{\text{PD}}(t)$ is derived in the Ref. [18], while the expression for $\mathcal{F}_{\text{AD}}(t)$ is more general than Ref. [2], since it includes the effect of the detuning δ . From the analytical expressions in Eqs. (11) and (12), we observe that variations on the components of the model parameter vector, ξ , will introduce different effects on the signal $f_m(t)$. Thus, estimating the SDF from data will depend on how sensitive the experimental signal is to variations on the vector ξ .

Previous works have been focused on antisymmetrized Lorentzian and Ohmic-like SDFs variations on expectation values in open quantum systems [16]. Thus, we only focus on quantifying the sensitivity in the AD model by considering a generic perturbation of the spectral density, $J(\omega) \mapsto J(\omega) + \delta J(\omega)$, and we study the induced change in the measured signal $f_{\text{AD}}(t) = 2|c_1(t)|^2 - 1$. At $T = 0$, the excited-state amplitude $c_1(t)$ obeys Eq. (7) with a bath-memory kernel $K(t) = \int_0^\infty J(\omega)e^{i(\omega-\omega_0)t}d\omega$. Therefore, the perturbation δJ enters only through $\delta K(t) = \int_0^\infty \delta J(\omega)e^{-i(\omega-\omega_0)t}d\omega$. Using the triangle inequality, we obtain the uniform bound $|\delta K(t)| \leq \int_0^\infty |\delta J(\omega)|d\omega \equiv \|\delta J\|_1$, where $\|x\|_1 := \int_0^\infty |x(\omega)|d\omega$ denotes the L^1 norm. Subtracting the two Volterra equations for $c_1(t)$ and $c_1(t) + \delta c_1(t)$, applying again the triangle inequality and a Grönwall-type estimate for Volterra integral equations, and finally using $|2|c_1 + \delta c_1|^2 - 2|c_1|^2| \leq 4|\delta c_1| + 2|\delta c_1|^2$ with $|c_1(t)|^2 \leq 1$, we arrive at the upper bound

$$|\Delta f_{\text{AD}}(t)| \leq 4t\|\delta J\|_1 \exp\left(\frac{t^2}{2}\|J\|_1\right), \quad (13)$$

where $\Delta f_{\text{AD}}(t) \equiv f_{\text{AD}}(t; J + \delta J) - f_{\text{AD}}(t; J)$ is the signal variation and $\|J\|_1 = \gamma_0 \lambda / (2\pi) [\pi/2 + \arctan \omega_b / \lambda]$. The above bound is valid for $t \geq 0$ and sufficiently small perturbations such that the quadratic term $2|\delta c_1(t)|^2$ is negligible, i.e., in the linear-response regime. Integrating Eq. (13) over a finite observation window $t \in [0, t_f]$, we obtain the L^1 -stability estimate of the accumulated error

$$\int_0^{t_f} |\Delta f_{\text{AD}}(t)| dt \leq \frac{4\|\delta J\|_1}{\|J\|_1} \left[\exp\left(\frac{\|J\|_1 t_f^2}{2}\right) - 1 \right]. \quad (14)$$

Equation (14) provides a worst-case upper bound of the experimental signal $f_{\text{AD}}(t)$ in terms of the integrated spectral perturbation. This is directly relevant for learning SDFs: it guarantees that small changes in $J(\omega)$, in the L^1 sense, cannot produce arbitrarily large deviations in the measured trace for finite times. However, the worst-case bound increases exponentially with the observation time, highlighting the intrinsic ill-conditioning of the inverse problem.

A. Simulated data and machine learning regressors

Simulated data for both PD and AD models are generated by sampling physical regimes in which the experimental signals (11) and (12) are well defined in the literature. To mimic experimental noise, we add multiplicative Gaussian fluctuations to each sampled point, $f_m(t_i) \rightarrow f_m(t_i) [1 + \delta_i]$. We set $\delta_i \sim \mathcal{N}(0, \sigma^2)$ independently for each t_i , and then clip the samples to a bounded interval $\delta_i \in [-\epsilon, \epsilon]$ to avoid rare outliers that would be nonphysical such as $\langle \sigma_z \rangle \notin [-1, 1]$. The simulated dataset for a given model is then $\mathcal{D}_m \equiv \{t_i, f_m(t_i) + \delta_i\}_{i=1}^N$. For parameter estimation, we develop a regression-based AI model by minimizing the cost function

$$\mathcal{L}_m = \frac{1}{N} \sum_{i=1}^N \left[\hat{f}(t_i, J(\omega; \xi)) - [f_m(t_i) (1 + \delta_i)] \right]^2, \quad (15)$$

where the maps (11) and (12) guide the optimization over ξ . Here, $\hat{f}(t_i, J(\omega, \xi))$ is the AI prediction of the experimental signal given a parametrized SDF. The optimal values in the ξ -landscape provide the best reconstruction of the real SDF. The computational methodology applies to both AD and PD channels, but for simplicity, we now focus on the AD model.

For the AD channel, we systematically benchmark several machine learning models, including support vector regression (SVR), multilayer perceptron (MLP), random forest (RF), extreme gradient boosting (XGBoost), and convolutional histogram-based gradient boosting regression tree (HistGBR). The training set comprised 9600 simulated instances with $n = 400$ data points for time, using $\omega_0 = 1$ as a dimensionless scale and parameters sampled uniformly within $[\omega_0/10, \omega_0]$ for $(\lambda, \gamma_0, \omega_b)$. To assess robustness, we considered two scenarios: (i) noiseless data ($\delta_i = 0$) and (ii) noisy data, where each experimental signal has a uniform random error with $\delta_i \in (0, 0.1)$ and $\langle \delta_i \rangle = 0.05$. The AI models are trained using a 75% and 25% split for training and testing, respectively, and we use k -fold cross-validation ($k = 5$) to optimize hyperparameters.

In Figure 2, we show the mean square error $\text{MSE} = M^{-1} \sum_{m=1}^M (\hat{y}_m^{\text{pred}} - \hat{y}_m^{\text{real}})^2$ and mean absolute error $\text{MAE} = M^{-1} \sum_{m=1}^M |\hat{y}_m^{\text{pred}} - \hat{y}_m^{\text{real}}|$ for the predicted \hat{y}_m^{pred} and real data \hat{y}_m^{real} . We calculate these metrics for both noisy and noiseless data when the real parameters $(\lambda, \gamma_0, \omega_b)$ are compared with the predictions. We observe that precision is approximately two orders of magnitude lower when noisy data is used to train AI regressors. Thus, in a realistic scenario, even a small amount of noise significantly reduces the precision of parameter estimation. In the next section, we will illustrate how to address this problem by using a structured bath environment as a target and combining theoretically inspired filtering techniques with neural network learning on noisy data.

IV. NEURAL NETWORK LEARNING WITH PRIOR COSINE TRANSFORM

When the SDF parametrization is unknown, neural networks (NNs) can be used as universal function approximators [22, 23]. Using a simulated dataset \mathcal{D}_m and the known quantum map, we can train a deep learning model to infer SDFs from dynamical signals, even in the presence of noise. We now focus on the PD model and the structured SDF $J(\omega) = J_{\text{bulk}}(\omega) + J_{\text{loc1}}(\omega) + J_{\text{loc2}}(\omega)$ [17], with

$$J_{\text{bulk}}(\omega) = 2\alpha \omega_c^{1-s} \omega^s e^{-\omega/\omega_c}, \quad (16)$$

$$J_{\text{loc1}}(\omega) = \frac{J_0 \omega^s}{(\omega/\omega_{\text{loc}} + 1)^2} \frac{\Gamma/2}{(\omega - \omega_{\text{loc}})^2 + (\Gamma/2)^2}, \quad (17)$$

$$J_{\text{loc2}}(\omega) = J_1 \omega^s e^{-(\omega - \omega_0)^2 / (2\sigma^2)}, \quad (18)$$

where $s = 3$, $\omega_c = 1$ THz, $\alpha = 0.0275$, $J_1 = 0.0025$ THz⁻², $\sigma = 2.4042$ THz, $\omega_0 = 9.35$ THz, $J_0 = 0.0235$ THz⁻¹, $\Gamma = 0.8414$ THz, and $\omega_{\text{loc}} = 15.19$ THz. The structured SDF accurately captures the electron-phonon coupling of the negatively charged silicon-vacancy center in diamond [8]. However, due to the complexity of the SDF (16)-(18), there is no analytical expression for the experimental signal $f_{\text{PD}}(t)$, only approximated expression due to the pronounced peak of $J_{\text{loc1}}(\omega)$ [8]. Now, the main idea is to find a linear integral transformation between the function $F(f_{\text{PD}}(t))$ and the SDF function $J(\omega)$, valid for any structured environment. Here, $F(\cdot)$ is a functional operator (to be discovered) acting on the signal $f_{\text{PD}}(t)$.

In the PD model, we note that the signal $H(t) = -d^2[\ln f_{\text{PD}}(t)]/dt^2$ with $f_{\text{PD}}(t) = C(0)\exp(-G(t))$ satisfy the linear integral relation with the SDF $J(\omega)$ since $H(t) = \int_0^\infty J(\omega) \coth(\beta\omega/2) \cos(\omega t) d\omega$, which resembles a cosine transform structure. Here, the operator $F(\cdot) = -d^2[\ln(\cdot)]/dt^2$. This motivates introducing the half-range cosine transform $\mathcal{C}\{f\}(\Omega) = \int_0^\infty f(t) \cos(\Omega t) dt$, which is a linear transformation since $\mathcal{C}\{\alpha_1 f_1 + \alpha_2 f_2\}(\Omega) = \alpha_1 \mathcal{C}\{f_1\}(\Omega) + \alpha_2 \mathcal{C}\{f_2\}(\Omega) \forall \alpha_i \in \mathbb{C}$ and $f_i(t)$ functions such that the cosine transform is well defined. Particularly, the inverse transform takes the form $\mathcal{C}^{-1}\{F\}(t) = (2/\pi) \int_0^\infty F(\Omega) \cos(\Omega t) d\Omega$, which is similar to the relation between $H(t)$ and $J(\omega)$. The latter yields the closed expres-

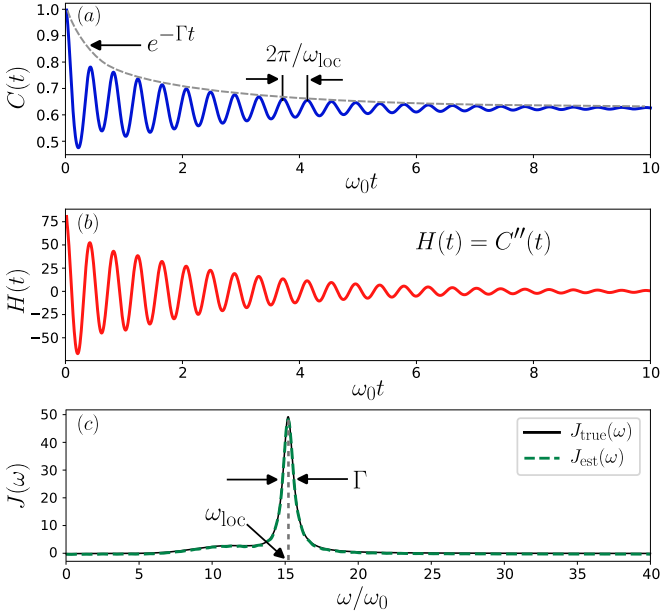


FIG. 3. Noise-free reconstruction using the discrete cosine transform. (a) Original coherence signal generated from the phenomenological SDF (Eqs. (16)-(18)). (b) Signal $H(t) = G''(t)$ used in the cosine transform (19). (c) True and estimated SDFs $J(\omega)$ using the discrete cosine transform, without machine learning processing.

sion

$$J(\Omega) = \frac{2}{\pi} \tanh\left(\frac{\beta\Omega}{2}\right) \mathcal{C}\left\{\frac{d^2G}{dt^2}\right\}(\Omega), \quad (19)$$

subject to the physical constraint $J(\Omega) \geq 0$. To derive Eq. (19), we have used the orthogonality relation $\int_0^\infty \cos(\omega t) \cos(\Omega t) dt = \pi \delta(\Omega - \omega)/2$, where $\delta(x)$ is the Dirac delta. Eq. (19) reveals a theoretical procedure to reconstruct the SDF from $d^2G/dt^2 = -C^{-1}(0)d^2[\ln f_{\text{PD}}(t)]/dt^2$ and the thermal factor $\tanh(\beta\Omega/2)$. However, experimental data is presented as discrete data points in time, including noise, as shown in the input of Fig. 2. To overcome this, we define an equally distributed discrete time grid $t_n = n\Delta t$ ($n = 0, \dots, N-1$, $t_f = N\Delta t$), where the Riemann sum $H_{t_f}(\nu_k) = \Delta t \sum_{n=0}^{N-1} H(t_n) \cos(\nu_k t_n)$ with $\nu_k = \pi k/t_f$ provides a discrete cosine transform estimate. We obtain

$$H_{t_f}(\nu) = \int_0^\infty J(\omega) \coth\left(\frac{\beta\omega}{2}\right) K_{t_f}(\nu, \omega) d\omega, \quad (20)$$

$$K_{t_f}(\nu, \omega) = \frac{\sin[(\nu - \omega)t_f]}{2(\nu - \omega)} + \frac{\sin[(\nu + \omega)t_f]}{2(\nu + \omega)}. \quad (21)$$

In the asymptotic limit $t_f \rightarrow \infty$ and in the absence of aliasing ($\omega_{\text{max}} < \pi/\Delta t$), this kernel reduces to $H_{t_f}(\nu) \simeq (\pi/2)J(\nu) \coth(\beta\nu/2)$, so the spectral peaks of $H_{t_f}(\nu)$ and $J(\nu)$ coincide up to thermal weighting. These observations motivate a frequency-domain preprocessing stage before applying a deep learning algorithm, but are physically inspired by the model. Naturally, for a different open quantum system, a linear integral relation $H(t) \mapsto J(\omega)$ must be derived, taking into account specific details of the model.

We then define the dataset $\mathcal{D}_\omega \equiv \{\mathcal{S}(\omega_n), \omega_n\}$ with $\mathcal{S}(\omega_n) = [2/(\pi \coth(\beta\omega_n/2))]H_T(\omega_n)$. Retaining dominant Fourier components $|\mathcal{S}(\omega_n)|^2$ provides a coarse reconstruction of $J(\omega)$ and a suitable starting guess of the SDF reconstruction, improving further neural network (NN) optimization. The NN is first pre-trained by minimizing the loss function (phase A)

$$\mathcal{L}_{\text{pre}} = \frac{1}{L} \sum_{n=1}^L [J_{\text{NN}}(\omega_n; \boldsymbol{\theta}) - \mathcal{S}(\omega_n)]^2, \quad (22)$$

yielding optimal NN parameters $\boldsymbol{\theta}^*$ after training and fine tuning. In a second postprocessing stage, the reconstruction of the SDF is refined using time domain information encoded in the signal $f_m(t)$, by minimizing the loss function (phase B)

$$\mathcal{L}_{\text{post}} = \frac{1}{N} \sum_{i=1}^N [\hat{f}_m(t_i, J_{\text{NN}}(\omega; \boldsymbol{\varphi})) - [f_m(t_i)(1 + \delta_i)]]^2, \quad (23)$$

initialized at $\boldsymbol{\varphi} = \boldsymbol{\theta}^*$ obtained in first pretraining (Phase A). Here, $\hat{f}_m(t_i, J_{\text{NN}}(\omega; \boldsymbol{\varphi}))$ is computed from the known quantum map $J(\omega) \mapsto f_m(t)$. Physical consistency is enforced by parametrizing

$$J_{\text{NN}}(\omega; \boldsymbol{\varphi}) = \mathcal{F}(\omega) [\mathbf{N}_J(\omega; \boldsymbol{\varphi})]^2, \quad (24)$$

with $\mathcal{F}(\omega) = \omega^d e^{-\omega/\Omega}$ representing a filter function, which guarantees the correct low- and high-frequency behavior. Here, $\mathbf{N}_J(\omega; \boldsymbol{\varphi})$ represent the NN prediction of the SDF in the Phase B. Equivalent constraints can be imposed using a softplus output layer in the NN or changing the filter function $\mathcal{F}(\omega)$ such that $\lim_{\omega \rightarrow 0, \infty} \mathcal{F}(\omega) = 0$. More details of the NN protocol is explained in Appendix B.

V. RESULTS OF SDF RECONSTRUCTION FOR THE PD MODEL USING NEURAL NETWORKS REFINEMENT

In the ideal noise-free setting (Fig. 3), the cosine transform in Eq. (19) already provides an accurate and parameter-free SDF reconstruction: it reproduces both the super-Ohmic envelope and the dominant localized features of $J(\omega)$ at negligible computational cost. This establishes a useful baseline: whenever the model is well known, and the signal-to-noise ratio is high, a linear inversion can provide a good approximation to the SDF without imposing a phenomenological SDF. This is more general than previous works [13–15], focusing on noise-free scenarios with phenomenological SDFs.

The situation changes in the presence of noise. We perturb the coherence as $C(t) \rightarrow C(t)[1 + \delta(t)]$ with $\max|\delta| = 5 \times 10^{-2}$ and $\langle \delta(t) \rangle = 0$, producing the signal observed in Fig. 4(a). The discrete cosine transform then yields a nonphysical SDF with multiple fictitious oscillations and negative regions, as shown in Fig. 4(b). The latter is expected from the second derivative sensitivity of $H(t) = -d^2[\ln f_{\text{PD}}(t)]/dt^2$ when finite-time windowing and noise are presented in $f_{\text{PD}}(t)$. We solve this issue by combining a cosine-based spectral prior (phase A) with a

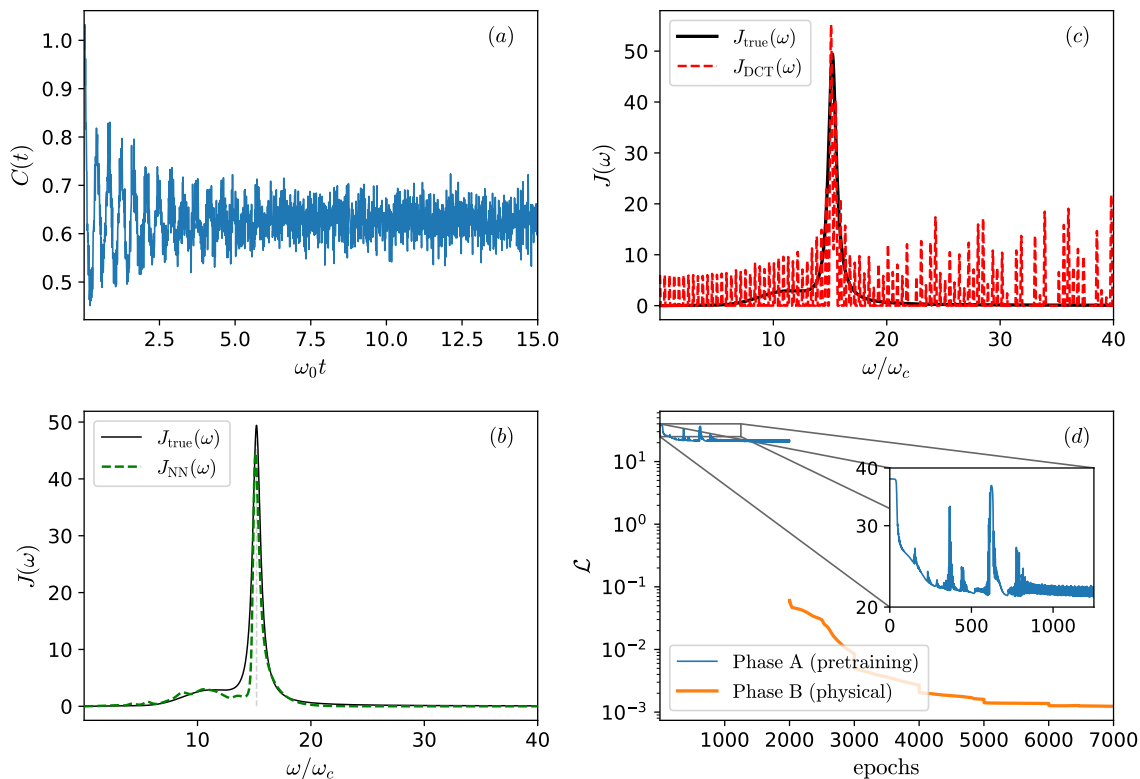


FIG. 4. Reconstruction of the SDF using a signal with 5% of noise in the coherence. (a) Original coherence for the phenomenological model including noise. (b) True and discrete cosine transform (DCT) SDFs. (c) Neural network reconstruction of the SDF using $J_{\text{DCT}}(\omega)$ in the preprocessing stage. (d) Loss function convergence for the two states: preprocessing (phase A) and postprocessing (phase B). Phase B corresponds to the learning of the SDF via a neural network.

physics-constrained NN refinement (phase B) that enforces non-negativity and corrects low- and high-frequency behavior while remaining consistent with the open dynamics. The resulting NN prediction is the SDF $J_{\text{NN}}(\omega)$, which is shown in Fig. 4(c) and compared with the original SDF. Most importantly, using the NN refinement, we obtain a smooth function that exhibits the main properties of the real structured bosonic bath. The convergence of the loss function in each phase (A and B) is illustrated in Fig. 4(d), where Phase B improves the learning of the SDF.

These results show that the ill-conditioned inverse problem of estimating the SDF from noisy time-dependent signals can be computationally solved by combining theoretical linear maps with deep learning-based refinement. However, the model plays a fundamental role in constructing the filtering functions and will depend on the particular open dynamics. Two intrinsic numerical limitations remain: low-frequency recovery is suppressed by the thermal factor $\tanh(\beta\omega/2)$, and finite acquisition time; overly strong smoothness regularization can wash out very narrow resonances.

VI. CONCLUSIONS

We developed and benchmarked two complementary, data-driven routes to reconstruct spectral density functions in exactly solvable open quantum models. Inverting time-domain signals to obtain frequency-dependent SDFs is an ill-conditioned problem. Small perturbations in the data can lead to large deviations in the reconstructed spectra. This behavior is expected for compact integral operators (see Ref [16] for related bounds).

In the parametric regime, regression techniques provide fast, interpretable estimates of SDF parameters, along with quantitative robustness maps against noise. However, this route assumes prior knowledge of the phenomenological models that describe the open dynamics. In the nonparametric regime, we showed that the cosine-transform structure of the quantum map induces a physics-consistent spectral prior whenever the signal-to-noise ratio is sufficiently high. Beyond this limit, a physics-constrained neural-network refinement, initialized by this prior and enforcing positivity and correct asymptotics, acts as a structured regularization mechanism, stabilizing the inversion and preserving the dominant spectral features under realistic noise and finite-time sampling.

From a mathematical perspective, the quantum map between dynamical observables and the SDF involves a in-

tegral relations, which defines a compact operator in frequency space. As a consequence, its inversion amplifies high-frequency components, rendering the problem intrinsically ill-conditioned under finite-time sampling and noisy data. The cosine-based prior and the constrained neural-network refinement, therefore, act as complementary regularization mechanisms, restoring stability while preserving physical consistency. These results establish a practical, scalable framework for environmental spectroscopy of structured reservoirs on solid-state platforms. More broadly, they provide a way to learn microscopic open quantum system models whenever known quantum maps are available.

ACKNOWLEDGMENTS

F.P., J.V.S.K.L., P.M.P. and F.F.F. acknowledge support from Fundação de Amparo à Pesquisa do Estado de São Paulo (FAPESP), project numbers 2024/20249-8, 2024/15741-0, 2025/08578-9 and 2023/04987-6. A.N. acknowledges the financial support from the project Fondecyt Regular No. 1251131 and ANID Anillo Project ATE250066.

Appendix A: GKSL derivation and dependence on the SDF

The starting point of the theory of open quantum systems is the Hamiltonian of the full (closed) system

$$\hat{H} = \hat{H}_s \otimes \mathbb{1}_b + \mathbb{1}_s \otimes \hat{H}_b + \hat{V}, \quad (\text{A1})$$

with $\hat{H}_s = \sum_a \hbar \omega_a |a\rangle\langle a|$, $\hat{H}_b = \sum_k \hbar \omega_k \hat{a}_k^\dagger \hat{a}_k$, and $\hat{V} = \hat{S} \hat{X}^\dagger + \hat{S}^\dagger \hat{X}$. Here, we are only considering a collective bath operator of the form $\hat{X} = \sum_k g_k \hat{a}_k$, where g_k encodes the system-bath couplings. For initially uncorrelated states $\hat{\rho}(0) = \hat{\rho}_s(0) \otimes \hat{\sigma}_b$, we assume a bath density matrix in thermal equilibrium

$$\hat{\sigma}_b = \frac{e^{-\beta \hat{H}_b}}{\text{Tr}[e^{-\beta \hat{H}_b}]}, \quad \beta = (k_B T)^{-1}, \quad (\text{A2})$$

which maximized the von Neumann entropy for a fixed average energy. Under the weak-coupling and secular approximations, the reduced state $\hat{\rho}_s(t) = \text{Tr}_b[\hat{\rho}(t)]$ follows the Gorini-Kossakowski-Sudarshan-Lindblad (GKSL) equation ($\hbar = 1$),

$$\begin{aligned} \dot{\hat{\rho}}_s = & -i[\hat{H}(t), \hat{\rho}_s(t)] + \sum_{\Omega} \sum_{n=1}^2 \gamma_n(t) \left[\hat{S}_n(\Omega) \hat{\rho}_s(t) \hat{S}_n^\dagger(\Omega) \right. \\ & \left. - \frac{1}{2} \{ \hat{S}_n^\dagger(\Omega) \hat{S}_n(\Omega), \hat{\rho}_s(t) \} \right]. \end{aligned} \quad (\text{A3})$$

Here, $\hat{H}(t)$ may include Lamb-shift corrections, and system operators in the frequency domain are defined as

$$\hat{S}_n(\Omega) = \sum_{a,b} \delta_k(\omega_{ba} - \Omega) |b\rangle\langle b| \hat{S}_n |a\rangle\langle a|, \quad (\text{A4})$$

where Ω is a frequency, $\hat{S}_1 = \hat{S}^\dagger$ and $\hat{S}_2 = \hat{S}$. The time-local damping rates are

$$\gamma_n(t) = 2 \int_0^\infty J(\omega) N_n(\omega) \frac{\sin[(\omega + \omega_n)t]}{\omega + \omega_n} d\omega, \quad (\text{A5})$$

with $N_1(\omega) = n(\omega)$, $N_2(\omega) = n(\omega) + 1$, $n(\omega) = \langle \hat{a}^\dagger(\omega) \hat{a}(\omega) \rangle_b$, and shifts $\omega_1 = \Omega$, $\omega_2 = -\Omega$. Thus, the reduced density matrix $\hat{\rho}_s(t)$ will naturally depend on the spectral density function $J(\omega)$, motivating the inverse problem of reconstructing the SDF from experimental observables $\langle \hat{O} \rangle = \text{Tr}_s[\hat{\rho}_S(t) \hat{O}]$.

Appendix B: Algorithmic protocol for reconstructing spectral density functions using cosine transform

In this appendix, we summarize the computational steps required to reproduce the reconstruction pipeline. All physical relations are defined in the main text, including the maps (Eqs. (11) and (12)) and the cosine-based estimator given in Eq. (19). No additional modeling assumptions are introduced.

a. Configuration. Fix the initial coherence $\rho_{eg}(0)$ and the temperature through $\beta = 1/(kT)$. Define time and frequency grids as $\{t_i\}_{i=0}^{N-1}$ and $\{\omega_j\}_{j=0}^{M-1}$, respectively. Record $(\Delta t, t_f, \Delta\omega, \omega_{\max})$. Set random seeds, numerical precision, and hardware configuration (e.g., float32 with or without mixed precision).

b. Preconditioning. Ensure $C(t) > 0$ before applying the logarithm. When required, clip the signal to a small threshold ε to prevent numerical underflow. Store the preconditioned signal together with all configuration metadata.

c. Cosine-based prior. Compute $G(t) = -\ln[C(t)/(2\rho_{eg}(0))]$ and evaluate its second derivative using consistent boundary stencils. Apply the half-range cosine transform to obtain $\mathcal{C}\{G''\}(\omega)$ and construct the spectral estimate $J_{\cos}(\omega)$ via Eq. (19), enforcing non-negativity. The resulting J_{\cos} is stored as a physics-informed spectral prior.

d. Neural-network refinement. Define $J_{\text{NN}}(\omega)$ using the physically constrained parameterization introduced in the main text. Initialize the network by minimizing \mathcal{L}_{pre} against $J_{\cos}(\omega)$, optionally including smoothness or curvature regularization in frequency. Subsequently refine the parameters by minimizing $\mathcal{L}_{\text{post}}$ using the maps (11)-(12). Early stopping or learning-rate scheduling may be employed. Store the optimal checkpoint and final parameters.

e. Diagnostics and outputs. Reconstruct the coherence $C_{\text{NN}}(t)$ from $J_{\text{NN}}(\omega)$ and generate side-by-side comparisons of $J_{\cos}(\omega)$, $J_{\text{NN}}(\omega)$, and, when available, the reference $J_{\text{true}}(\omega)$, as well as $C(t)$ versus $C_{\text{NN}}(t)$ (see Figs. 3 and 4). Archive checkpoints, grids, random seeds, unit conventions, and plotting scripts.

f. Robustness checks. Repeat the protocol for multiple random seeds and for moderate variations of $(kT, \rho_{10}(0))$ and windowing parameters to assess the stability of $J_{\text{NN}}(\omega)$ and the reconstructed coherence.

-
- [1] I. de Vega and D. Alonso, Dynamics of non-Markovian open quantum systems, *Rev. Mod. Phys.* **89**, 015001 (2017).
- [2] H.-P. Breuer and F. Petruccione, *The Theory of Open Quantum Systems* (Oxford University Press, Oxford, 2002).
- [3] A. O. Caldeira and A. J. Leggett, *Path integral approach to quantum Brownian motion*, *Physica A: Statistical Mechanics and its Applications* **121**, 587-616 (1983).
- [4] A. J. Leggett, S. Chakravarty, A. T. Dorsey, Matthew P. A. Fisher, Anupam Garg, and W. Zwerger, *Dynamics of the dissipative two-state system*, *Rev. Mod. Phys.* **59**, 1 (1987).
- [5] U. Weiss, *Quantum Dissipative Systems* (Scientific, Singapore, 2008).
- [6] I. Wilson-Rae and A. Imamolu, *Quantum dot cavity-QED in the presence of strong electron-phonon interactions*, *Phys. Rev. B* **65**, 235311 (2002).
- [7] A. Alkauskas, B. B. Buckley, D. D. Awschalom, and C. G. Van de Walle, First-principles theory of the luminescence lineshape for the triplet transition in diamond NV centres, *New J. Phys.* **16**, 073026 (2014).
- [8] A. Norambuena, S. A. Reyes, J. Meja-Lopez, A. Gali, and J. R. Maze, Microscopic modeling of the effect of phonons on the optical properties of solid-state emitters, *Phys. Rev. B* **94**, 134305 (2016).
- [9] F. J. Gonzalez, D. Tancara, H. T. Dinani, R. Coto, and A. Norambuena, Engineering non-Markovianity from defect-phonon interactions, *New J. Phys.* **25**, 043004 (2023).
- [10] M. C. Cambria, A. Norambuena, H. T. Dinani, G. Thiering, A. Gardill, I. Kemeny, Y. Li, V. Lordi, A. Gali, J. R. Maze, and S. Kolkowitz, Temperature-Dependent Spin-Lattice Relaxation of the Nitrogen-Vacancy Spin Triplet in Diamond, *Phys. Rev. Lett.* **130**, 256903 (2023).
- [11] A. Norambuena, E. Muoz, H. T. Dinani, A. Jarmola, P. Maletinsky, D. Budker, and J. R. Maze, Spin-lattice relaxation of individual solid-state spins, *Phys. Rev. B* **97**, 094304 (2018).
- [12] A. O. Caldeira and A. J. Leggett, Influence of dissipation on quantum tunneling in macroscopic systems, *Phys. Rev. Lett.* **46**, 211 (1981).
- [13] J. Barr, G. Zicari, A. Ferraro, and M. Paternostro, Spectral density classification for environment spectroscopy, *Mach. Learn.: Sci. Technol.* **5**, 015043 (2024).
- [14] J. Barr, S. Mukherjee, A. Ferraro, M. Paternostro, and G. Zicari, A machine learning based approach to the identification of spectral densities in quantum open systems, *arXiv:2507.13730* (2025).
- [15] J. Barr, S. Mukherjee, A. Ferraro, M. Paternostro, and G. Zicari, *Machine Learning-Enhanced Characterisation of Structured Spectral Densities: Leveraging the Reaction Coordinate Mapping*, *arXiv:2501.07485* (2025).
- [16] F. Mascherpa, A. Smirne, S. F. Huelga, and M. B. Plenio, Open Systems with Error Bounds: Spin-Boson Model with Spectral Density Variations, *Phys. Rev. Lett.* **118**, 100401 (2017).
- [17] A. Norambuena, J. R. Maze, P. Rabl, and R. Coto, Quantifying phonon-induced non-Markovianity in color centers in diamond, *Phys. Rev. A* **101**, 022110 (2020).
- [18] P. Haikka, T. H. Johnson, and S. Maniscalco, Non-Markovianity of local dephasing channels and time-invariant discord, *Phys. Rev. A* **87**, 010103(R) (2013).
- [19] J. Luczka, *Spin in contact with thermostat: Exact reduced dynamics*, *Physica A* **167**, 919 (1990).
- [20] T. Baumgratz, M. Cramer, and M. B. Plenio, *Quantifying Coherence*, *Phys. Rev. Lett.* **113**, 140401 (2014)
- [21] T. Jacob, *Understanding the Lomb-Scargle Periodogram*, *ApJS* **236** 16 (2018).
- [22] G. Cybenko, *Approximation by superpositions of a sigmoidal function*, *Math. Control Signals Syst.* **2**, 303 (1989).
- [23] K. Hornik, *Approximation capabilities of multilayer feedforward networks*, *Neural Networks* **4**, 251 (1991).